Properties of deformed even-even nuclei near $Z = 20$ in an improved quark mass density-dependent model

Renli Xu (徐仁力),[1,*] Chen Wu (吴琛),[2,†] Guoliang Ma (马国亮),[2] Deqing Fang (方德清),[2] and Zhongzhou Ren (任中洲)[1,3,‡]
[1]*Department of Physics, Nanjing University, Nanjing 210093, People's Republic of China*
[2]*Shanghai Institute of Applied Physics, Chinese Academy of Sciences, Shanghai 201800, People's Republic of China*
[3]*Center of Theoretical Nuclear Physics, National Laboratory of Heavy-Ion Accelerator, Lanzhou 730000, People's Republic of China*
(Received 16 October 2012; revised manuscript received 10 December 2012; published 24 January 2013)

An improved quark mass density-dependent model is applied to study the ground-state properties of axially deformed even-even nuclei using the deformed quark-meson coupling calculation. The present study is mainly focused on the nuclei with the available experimental data ranging from $Z = 14$ to $Z = 26$. The ground-state binding energies, two-neutron separation energies, two-proton separation energies, quadrupole deformations, and root-mean-square (rms) charge radii are studied. The shell effect of the neutron magic number $N = 20$ can be demonstrated by our model. It has been shown that the improved quark mass density-dependent model can give a reasonable description of the axially deformed nuclei.

DOI: 10.1103/PhysRevC.87.014335 PACS number(s): 21.10.Gv, 21.60.−n, 24.70.+s, 25.30.Bf

I. INTRODUCTION

Relativistic calculations of finite nuclei and infinite nuclear matter play important roles in theoretical nuclear physics. It is known that quantum chromodynamics (QCD) is very difficult to study in a nuclear system directly because of its nonperturbative nature, so phenomenological models reflecting the characteristics of the strong interaction are widely used in research of the properties of nuclear matter and finite nuclei. The relativistic mean field (RMF) model based on baryon and meson degrees of freedom gives a reasonable starting point for the studies of nuclear matter as well as the physical properties of finite nuclei [1–6]. Meanwhile, many effective models based on quark and meson degrees of freedom have also been proposed. They include the quark meson coupling (QMC) model [7–9], the chiral SU(3) quark model [10–12], the quark mean field model [13], and the improved quark mass density-dependent (IQMDD) model [14]. Among these models, the QMC and IQMDD models are hybrid quark-meson models based on bag models of nucleons. The famous QMC model, first suggested by Guichon [7] in 1988, describes nuclear matter as a collection of nonoverlapping MIT bags, scalar σ mesons and vector ω mesons [15]. Meanwhile, the IQMDD model [14] constructs the Friedberg-Lee (FL) soliton bag in a nuclear system after introducing the nonlinear interaction of σ mesons and $qq\sigma$ coupling, which replaces the permanent confinement mechanism (MIT bag) in the QMC model with a nonpermanent confinement mechanism (FL soliton bag [16]). Both the QMC model and the IQMDD model can describe many physical properties of nuclear matter and spherical nuclei successfully.

There are lots of work about deformed relativistic mean-field calculations based on baryon and meson degrees of freedom [17–21], while the deformed calculation based on quark and meson degrees of freedom has not been studied yet. The motivation of this paper is to extend the improved quark mass density-dependent (IQMDD) model [14] to describe the deformed nuclei. The IQMDD model, where mesons couple only to the quarks, is derived from the quark mass density-dependent(QMDD) model [22,23] by Wu and his collaborators. The IQMDD model provides natural coupling constants between mesons and quarks. Meanwhile, some investigations indicate that the traditional hadronic physics approach may have its limitations [8]. In Refs. [8,24,25], it was concluded that when the naive dimensional analysis (NDA) was applied to quantum hadrodynamics (QHD), the relativistic Hartree approximation (RHA) in QHD leads to unnaturally large coefficients due to the treatment of the vacuum in terms of the excitation of $N\overline{N}$ pairs. On the other hand, alternative approaches which include subhadronic degrees of freedom may give some different insights into the properties of finite nuclei and nuclear matter. Under the mean field approximation, the effective nucleon mass in the IQMDD model has a nonlinear relationship with the σ field rather than RMF model (the result is also same for the QMC model).

According to the QMDD model, suggested by Fowler, Raha, and Weiner, the masses of u, d quarks and strange quarks (and the corresponding antiquarks) are given by

$$m_q = \frac{B}{3n_B}(q = u, d, \bar{u}, \bar{d}), \tag{1}$$

$$m_{s,\bar{s}} = m_{s0} + \frac{B}{3n_B}, \tag{2}$$

where n_B is the baryon number density, m_{s0} is the current mass of the strange quark, and B is the bag constant. In the IQMDD model where the σ, ω, and ρ mesons are added, the quark masses are still density dependent. The interactions between quarks and mesons are extended to the whole system. The IQMDD model can successfully describe the quark deconfinement phase transition [26,27] and carry out nuclear many-body calculations beyond the mean field approximation (MFA) in principle [28].

*xurenli.phy@gmail.com
†Corresponding author: wuchenoffd@gmail.com
‡zren@nju.edu.cn

Seven isotopic chains near $Z = 20$ are investigated in this paper. Additionally, we also calculate these nuclei with the RMF parameter sets NL3 [2] and FSU [3] for comparison. Usually, the MFA is thought to be reliable for describing ground-state properties of nuclei with mass number A around and larger than 40. Our studied nuclei are just in the lower limit of validity for such an approach and there are many experimental deformed isotopes in this region, so it is interesting to use deformed calculations based on quark and meson degrees of freedom to investigate these nuclei and test their validity and reliability for describing the properties of deformed nuclei. After writing down the Lagrangian density for finite nuclei at the hadronic level, the Dirac equation for nucleons and the Klein-Gordon equations for meson fields and the photon field can be obtained. For the deformed calculation, we expand the Dirac spinors as well as the meson fields in terms of oscillator wave functions in cylindrical coordinates. The set of coupled partial differential equations can be solved self-consistently. Then we calculate the ground-state properties of even-even nuclei from $Z = 14$ to 26. In this region, there are plenty of experimental data available. We emphasize that we are the first to apply deformed relativistic mean-field calculations based on quark and meson degrees of freedom to investigate these isotopic chains. Our model can well describe the studied properties of these finite nuclei.

The organization of this paper is as follows. In Sec. II, the theoretical framework for finite nuclei in the IQMDD model is given. The model parameters and the calculated results are presented and discussed in Sec. III. Finally, a summary is given in Sec. IV.

II. FORMULAS OF THE IQMDD MODEL FOR FINITE NUCLEI

In the IQMDD model, the effective Lagrangian density is written as

$$\begin{aligned}\mathcal{L} = {} & \bar{\varphi}\left[\gamma^{\mu}\left(i\partial_{\mu} - g^{q}_{\omega}\omega_{\mu} - \frac{g^{q}_{\rho}}{2}\tau\rho_{\mu}\right) - m_{q} + g^{q}_{\sigma}\sigma\right]\varphi \\ & + \frac{1}{2}\partial^{\mu}\sigma\,\partial_{\mu}\sigma - U(\sigma) - \frac{1}{4}F^{\mu\nu}F_{\mu\nu} + \frac{1}{2}m^{2}_{\omega}\omega^{\mu}\omega_{\mu} \\ & - \frac{1}{4}G^{\mu\nu}G_{\mu\nu} + \frac{1}{2}m^{2}_{\rho}\rho^{\mu}\rho_{\mu}. \end{aligned} \tag{3}$$

The strength tensors of the vector mesons are defined as $F_{\mu\nu} = \partial_{\mu}\omega_{\nu} - \partial_{\nu}\omega_{\mu}$, $G_{\mu\nu} = \partial_{\mu}\rho_{\nu} - \partial_{\nu}\rho_{\mu}$, the quark mass m_q is given by Eqs. (1) and (2), and g^{q}_{σ}, g^{q}_{ω}, and g^{q}_{ρ} are the coupling constants between the quark-σ meson, quark-ω meson, and quark-ρ meson, respectively. $U(\sigma)$ is the self-interaction potential for the σ field, which has the form

$$U(\sigma) = \tfrac{1}{2}m^{2}_{\sigma}\sigma^{2} + \tfrac{1}{3}b\sigma^{3} + \tfrac{1}{4}c\sigma^{4} + B. \tag{4}$$

The bag constant B is introduced so that

$$U(\sigma_{v}) = 0, \quad U(0) = B, \tag{5}$$

thus

$$\begin{aligned} -B &= \frac{1}{2}m^{2}_{\sigma}\sigma^{2}_{v} + \frac{1}{3}b\sigma^{3}_{v} + \frac{1}{4}c\sigma^{4}_{v}, \\ \sigma_{v} &= \frac{-b}{2c}\left(1 + \sqrt{1 - 4m^{2}_{\sigma}c/b^{2}}\right), \end{aligned} \tag{6}$$

where σ_v is the σ field value when $U(\sigma)$ has the absolute minimum. The equation of motion for the quark field under the MFA in the whole space is

$$\left[i\gamma^{\mu}\partial_{\mu} - \left(m_{q} - g^{q}_{\sigma}\sigma\right) - g^{q}_{\omega}\gamma^{0}\omega_{0} - \frac{g^{q}_{\rho}}{2}\gamma^{0}\tau_{3}\rho_{0}\right]\varphi = 0. \tag{7}$$

The effective quark mass m^{*}_{q} is given by

$$m^{*}_{q} = m_{q} - g^{q}_{\sigma}\sigma. \tag{8}$$

In nuclear matter, three quarks constitute a FL soliton bag, and the effective nucleon mass is obtained from the bag energy and reads

$$\begin{aligned} M^{*}_{N} &= \sum_{q} E_{q} \\ &= \sum_{q} \frac{4}{3}\pi R^{3}\frac{\Gamma_{q}}{(2\pi)^{3}}\int_{0}^{K^{q}_{F}} \sqrt{m^{*2}_{q} + k^{2}}\left(\frac{dN_{q}}{dk}\right)dk, \end{aligned} \tag{9}$$

where Γ_q is the quark degeneracy, K^{q}_{F} is the Fermi energy of quarks, and $\sum_q$ denotes the summation for quarks. dN_q/dk is the density of states for various quarks in a spherical cavity. The expressions of dN_q/dk and K^{q}_{F} adopted in this paper can be found in Ref. [29]. Using the equilibrium condition for the nucleon bag, the bag radius R can be determined by

$$\frac{\delta M^{*}_{N}}{\delta R} = 0. \tag{10}$$

We note that the expression of the effective nucleon mass for IQMDD is different from that of the RMF model (FSU, NL3). Let us consider the self-consistency condition and $(\frac{\partial M^{*}_{N}}{\partial\sigma})_{R}$ further. Using the same argument as that of Ref. [15], the $(\frac{\partial M^{*}_{N}}{\partial\sigma})_{R}$ can be expressed as

$$\left(\frac{\partial M^{*}_{N}}{\partial\sigma}\right)_{R} = -g_{\sigma} \times \begin{pmatrix} 1 \\ c(\sigma) \end{pmatrix} \text{for} \begin{pmatrix} \text{NL3, FSU} \\ \text{IQMDD} \end{pmatrix}, \tag{11}$$

where $c(\sigma)$ is the scalar density factor. More detailed discussion about it can be found in Ref. [14]. For investigating the finite nuclei, one can construct a relativistic Lagrangian density at the hadronic level under the MFA in the following form:

$$\begin{aligned} \mathcal{L}_{\text{RMF}} = {} & \bar{\psi}\Big[i\gamma^{\mu}\partial_{\mu} - M^{*}_{N}(\sigma) - g_{\omega}\gamma^{0}\omega_{0}(\mathbf{r}) - \frac{g_{\rho}}{2}\gamma^{0}\tau_{3}\rho_{0}(\mathbf{r}) \\ & - \frac{e}{2}\gamma^{0}(1 + \tau_{3})A_{0}(\mathbf{r})\Big]\psi - \frac{1}{2}[\nabla\sigma(\mathbf{r})]^{2} - U(\sigma) \\ & + \frac{1}{2}\left\{[\nabla\omega_{0}(\mathbf{r})]^{2} + m^{2}_{\omega}\omega_{0}(\mathbf{r})^{2}\right\} \\ & + \frac{1}{2}\left\{[\nabla\rho_{0}(\mathbf{r})]^{2} + m^{2}_{\rho}\rho_{0}(\mathbf{r})^{2}\right\} + \frac{1}{2}[\nabla A_{0}(\mathbf{r})]^{2}, \end{aligned} \tag{12}$$

where ψ's are the Dirac spinors for the nucleons and A_0 denotes the electromagnetic field. The coupling constants between nucleon and ω meson, ρ meson are chosen as $g_{\omega} = 3g^{q}_{\omega}$ and $g_{\rho} = g^{q}_{\rho}$ [15]. Using the Euler-Lagrange equation we obtain the Dirac equation for nucleons as follows:

$$\begin{aligned} & \Big[i\gamma^{\mu}\partial_{\mu} - M^{*}_{N} - g_{\omega}\gamma^{0}\omega_{0}(\mathbf{r}) - \frac{g_{\rho}}{2}\gamma^{0}\tau_{3}\rho_{0}(\mathbf{r}) \\ & - \frac{e}{2}\gamma^{0}(1 + \tau_{3})A_{0}(\mathbf{r})\Big]\psi = 0. \end{aligned} \tag{13}$$

The Klein-Gordon equations for the mesons and photon can be written as

$$\left(-\Delta + m_\sigma^2\right)\sigma(\mathbf{r}) = -\frac{\partial M_N^*}{\partial \sigma}\rho_s(\mathbf{r}) - b\sigma^2(\mathbf{r}) - c\sigma^3(\mathbf{r}), \quad (14)$$

$$\left(-\Delta + m_\omega^2\right)\omega_0(\mathbf{r}) = g_\omega \rho_v(\mathbf{r}), \quad (15)$$

$$\left(-\Delta + m_\rho^2\right)\rho_0(\mathbf{r}) = \frac{g_\rho}{2}\rho_3(\mathbf{r}), \quad (16)$$

$$-\Delta A_0(\mathbf{r}) = e\rho_p(\mathbf{r}), \quad (17)$$

where ρ_s, ρ_v, ρ_3, and ρ_p are the densities of scalar, baryon, third component of isovector, and proton, respectively. These source densities can be expressed as

$$\rho_s(\mathbf{r}) = \sum_{i=1}^{A} \bar{\psi}_i(\mathbf{r})\psi_i(\mathbf{r}), \quad (18)$$

$$\rho_v(\mathbf{r}) = \sum_{i=1}^{A} \psi_i^+(\mathbf{r})\psi_i(\mathbf{r}), \quad (19)$$

$$\rho_3(\mathbf{r}) = \sum_{p=1}^{Z} \psi_p^+(\mathbf{r})\psi_p(\mathbf{r}) - \sum_{n=1}^{N} \psi_n^+(\mathbf{r})\psi_n(\mathbf{r}), \quad (20)$$

$$\rho_p(\mathbf{r}) = \sum_{p=1}^{Z} \psi_p^+(\mathbf{r})\psi_p(\mathbf{r}). \quad (21)$$

The above coupled equations (13)–(17) can be self-consistently solved with the effective mass of nucleon obtained by Eq. (9). In this work, we calculate the ground-state properties of even-even nuclei near $Z = 20$ and use the BCS method to deal with the pairing interactions.

III. NUMERICAL RESULTS AND DISCUSSION

First, let us discuss the parameters in the IQMDD model. As those of Refs. [14], the masses of ω meson, ρ meson, and σ meson are fixed as $m_\omega = 783$ MeV, $m_\rho = 770$ MeV, and $m_\sigma = 509$ MeV. We get the bag constant $B = 174$ MeV fm^{-3} to fit the nucleon mass as $M_N = 939$ MeV. In order to get the compression constant $K(\rho_0) = 210$ MeV and the binding energy per particle $E/A = -15.0$ MeV at the nuclear saturation density $\rho_0 = 0.15$ fm^{-3}, we fix $g_\omega^q = 2.44$, $g_\sigma^q = 4.67$, and $b = -1460$ MeV, and the coupling constant c can be deduced from Eq. (6). In addition, we fix $g_\rho^q = 9.07$ to get a modest symmetry energy coefficient as about 33.2 MeV.

There have been some investigations on the even-even nuclei near $Z = 20$ [17]. In Ref. [17], Lalazissis *et al.* studied the properties of these nuclei with NL3 [2]. Their calculations show that the RMF model is valid and reliable for describing the properties of the nuclei in this region. In the present work, we apply the IQMDD model to study these nuclei.

We follow the same method of oscillator base expansion as described in Ref. [30]. The number of oscillator shells in our calculation is chosen as $N_f = N_b = 12$. With the BCS approximations, the pairing correlation is taken into account for these even-even nuclei. The constant pairing gaps are taken with the following forms [31,32]:

$$\Delta_n = \frac{4.8}{N^{1/3}}\text{MeV}, \quad \Delta_p = \frac{4.8}{Z^{1/3}}\text{MeV}, \quad (22)$$

where N and Z are the neutron and the proton numbers, respectively. These effective-interaction pairing gaps were determined by least-squares minimization comparing to the calculated paring gaps for experimental odd-even mass differences, and the root-mean-square (rms) deviation of the result with these pairing gaps are lower than that of the conventional form const/$\sqrt{A}$ [31]. An axial deformation is assumed initially for the iteration in the calculation. It stressed that the different selections of the deformation parameter β_0 lead to different iteration numbers of the self-consistent calculation and different computational time. Physical quantities such as the binding energy and the deformation do not change much. The whole calculation is performed with the range of the deformation β_0 from -0.5 to 0.5, with the steps of 0.1. This can guarantee the reliability of the numerical results in deformed IQMDD calculations. The charge radius is taken as $R_c = \sqrt{R_p^2 + 0.64}$ fm, where R_p is the rms radius of the proton distribution.

The calculated binding energy per nucleon E/A, quadrupole deformations β_2, and various rms radii are listed in Table I. Hexadecupole moments H are also listed there since they are important in transitional nuclei [33]. For comparison, the experimental values for the binding energy per nucleon and quadrupole deformation taken from Ref. [34,35] are also included. For a better understanding of the agreement between theory and experiment, we discuss our calculated results in detail.

We plot the binding energy as functions of the mass numbers for S, Ar, Ca, and Cr in Fig. 1. The results calculated with the RMF model (NL3, FSU) are also included for comparison. The squares, diamonds, stars, and open circles are respectively the experimental data taken from Ref. [34] and the calculated results with FSU, NL3, and IQMDD. It can be seen from Fig. 1 that calculated binding energies per particle with IQMDD are smaller in absolute value than the results with FSU, NL3, and experimental values. However, they have the same change trend with the mass number increasing. Besides, as we see in Fig. 1, the calculated binding energies for ^{36}S, ^{38}Ar, and ^{52}Cr have the largest values in their respective isotopic chains, which correspond to the neutron magic number $N = 20, 28$. Meanwhile, in our calculation, the rms deviation of the total binding energies in IQMDD with respect to the experimental data for the nuclei presented in Table I is about 12 MeV, while the rms deviation of the total binding energies for these nuclei in NL3 is about 3 MeV, and the result for FSU is slightly larger than NL3. In the IQMDD model, we fit the binding energy per particle $E/A = -15.00$ MeV at the nuclear saturation density $\rho_0 = 0.150$ fm^{-3}, while $E/A = -16.30$ MeV at the nuclear saturation density $\rho_0 = 0.148$ fm^{-3} for NL3 [2] and for FSU [3], which is one of the main reasons why the IQMDD model gives smaller binding energies than the experimental data.

The quadrupole deformation parameter β_2, which is an important quantity for describing the nuclear shape, can be obtained by solving the deformed IQMDD equations. While the experimental values of quadrupole deformation parameter β in Ref. [35] are given as

$$\beta = \left(4\pi/3ZR_0^2\right)[B(E2)\uparrow/e^2]^{1/2}, \quad (23)$$

TABLE I. Binding energy per baryon, E/A (in MeV), rms radii of the neutron (R_n) and proton (R_p), rms charge radius (R_c) (in fm), and quadrupole deformation and total hexadecupole moment of even-even nuclei near $Z = 20$ with IQMDD. The available experimental data in the last two columns are taken from the nuclear mass table [34] and Ref. [35].

Nucleus	IQMDD						Expt	
	E/A	R_n	R_p	R_c	β_2	$H(b^2)$	E/A	β
^{24}Si	−6.95	2.93	3.27	3.37	0.490	0.011	−7.17	
^{26}Si	−7.60	3.07	3.24	3.34	0.569	0.011	−7.92	0.446
^{28}Si	−8.02	3.19	3.23	3.33	0.580	0.005	−8.45	0.407
^{30}Si	−8.08	3.25	3.19	3.29	0.447	0.001	−8.52	0.315
^{32}Si	−8.16	3.29	3.15	3.25	−0.275	0.006	−8.48	0.217
^{34}Si	−8.15	3.34	3.12	3.22	−0.005	0.000	−8.34	0.179
^{36}Si	−7.91	3.48	3.17	3.27	0.216	0.016	−8.11	0.259
^{38}Si	−7.72	3.62	3.24	3.34	0.401	0.040	−7.89	0.249
^{40}Si	−7.53	3.74	3.30	3.39	0.489	0.043	−7.66	
^{42}Si	−7.29	3.84	3.33	3.43	0.498	0.027	−7.37	
^{28}S	−7.15	3.06	3.35	3.44	0.451	0.007	−7.48	
^{30}S	−7.70	3.15	3.29	3.39	0.456	0.019	−8.12	0.338
^{32}S	−8.05	3.21	3.26	3.35	0.315	0.011	−8.49	0.312
^{34}S	−8.30	3.27	3.23	3.33	−0.248	0.000	−8.58	0.252
^{36}S	−8.39	3.32	3.20	3.30	−0.004	0.000	−8.58	0.168
^{38}S	−8.22	3.45	3.23	3.33	0.110	0.007	−8.45	0.246
^{40}S	−8.08	3.57	3.28	3.38	0.298	0.029	−8.33	0.284
^{42}S	−7.93	3.68	3.33	3.43	0.386	0.034	−8.19	0.300
^{44}S	−7.75	3.77	3.37	3.46	0.407	0.021	−7.99	0.254
^{46}S	−7.56	3.86	3.39	3.49	0.393	−0.005	−7.78	
^{32}Ar	−7.39	3.13	3.36	3.46	−0.286	0.006	−7.70	
^{34}Ar	−7.91	3.20	3.33	3.42	−0.252	0.001	−8.20	0.238
^{36}Ar	−8.30	3.26	3.31	3.41	−0.212	0.000	−8.52	0.256
^{38}Ar	−8.53	3.32	3.28	3.38	−0.007	0.000	−8.61	0.163
^{40}Ar	−8.45	3.43	3.29	3.39	−0.004	0.001	−8.60	0.251
^{42}Ar	−8.32	3.53	3.33	3.42	0.142	0.008	−8.56	0.275
^{44}Ar	−8.21	3.63	3.36	3.45	0.244	0.015	−8.49	0.240
^{46}Ar	−8.10	3.72	3.39	3.49	0.285	0.027	−8.41	0.175
^{48}Ar	−7.98	3.80	3.42	3.51	−0.273	0.027	−8.27	
^{50}Ar	−7.85	3.88	3.45	3.54	−0.276	0.019	−8.08	
^{36}Ca	−7.63	3.18	3.39	3.49	−0.004	0.000	−7.82	
^{38}Ca	−8.15	3.25	3.37	3.47	−0.007	0.001	−8.24	0.125
^{40}Ca	−8.52	3.32	3.37	3.46	−0.005	0.001	−8.55	0.123
^{42}Ca	−8.53	3.42	3.37	3.47	−0.004	0.000	−8.62	0.247
^{44}Ca	−8.46	3.51	3.39	3.48	−0.005	0.000	−8.66	0.253
^{46}Ca	−8.40	3.59	3.40	3.50	−0.006	0.000	−8.67	0.153
^{48}Ca	−8.32	3.66	3.42	3.51	−0.011	0.000	−8.67	0.106
^{50}Ca	−8.23	3.74	3.45	3.54	−0.058	0.004	−8.55	
^{52}Ca	−8.15	3.81	3.47	3.56	0.100	0.000	−8.40	
^{54}Ca	−8.05	3.88	3.49	3.58	−0.070	0.000	−8.22	
^{56}Ca	−7.95	3.94	3.51	3.60	0.000	0.000	−8.03	
^{40}Ti	−7.72	3.27	3.51	3.60	−0.006	0.000	−7.86	
^{42}Ti	−8.18	3.33	3.49	3.58	−0.005	0.000	−8.26	0.319
^{44}Ti	−8.28	3.43	3.49	3.58	−0.011	0.000	−8.53	0.268
^{46}Ti	−8.38	3.55	3.52	3.61	0.255	0.078	−8.66	0.317
^{48}Ti	−8.41	3.64	3.54	3.63	0.311	0.081	−8.72	0.269
^{50}Ti	−8.40	3.71	3.56	3.64	0.311	0.062	−8.76	0.166
^{52}Ti	−8.35	3.77	3.56	3.65	0.265	0.032	−8.69	
^{54}Ti	−8.30	3.82	3.57	3.65	0.205	0.011	−8.60	
^{56}Ti	−8.24	3.87	3.58	3.67	0.137	0.016	−8.46	
^{58}Ti	−8.17	3.93	3.59	3.68	−0.091	0.000	−8.31	
^{60}Ti	−8.09	3.99	3.60	3.69	0.002	0.000	−8.15	
^{42}Cr	−7.26	3.30	3.63	3.72	0.159	0.011	−7.48	
^{44}Cr	−7.77	3.35	3.59	3.68	−0.004	0.002	−7.95	

TABLE I. (*Continued.*)

Nucleus	IQMDD						Expt	
	E/A	R_n	R_p	R_c	β_2	$H(b^2)$	E/A	β
^{46}Cr	−8.03	3.47	3.61	3.70	0.257	0.081	−8.30	
^{48}Cr	−8.23	3.58	3.63	3.72	0.339	0.106	−8.57	0.337
^{50}Cr	−8.36	3.67	3.65	3.74	0.397	0.110	−8.70	0.293
^{52}Cr	−8.41	3.73	3.66	3.75	0.391	0.089	−8.77	0.223
^{54}Cr	−8.41	3.79	3.67	3.75	0.354	0.056	−8.78	0.250
^{56}Cr	−8.39	3.84	3.67	3.75	0.303	0.028	−8.72	
^{58}Cr	−8.36	3.88	3.67	3.75	0.228	0.035	−8.64	
^{60}Cr	−8.31	3.93	3.67	3.76	0.138	0.008	−8.53	
^{62}Cr	−8.25	3.98	3.67	3.76	0.033	0.000	−8.42	
^{64}Cr	−8.18	4.05	3.69	3.78	0.011	0.000	−8.30	
^{66}Cr	−8.00	4.13	3.71	3.80	0.020	0.000	−8.16	
^{50}Fe	−8.02	3.60	3.74	3.82	0.403	0.115	−8.35	
^{52}Fe	−8.24	3.70	3.75	3.84	0.443	0.117	−8.61	
^{54}Fe	−8.35	3.76	3.76	3.84	0.430	0.094	−8.74	0.195
^{56}Fe	−8.41	3.81	3.76	3.84	0.401	0.059	−8.79	0.239
^{58}Fe	−8.43	3.86	3.76	3.84	0.360	0.029	−8.79	0.258
^{60}Fe	−8.42	3.90	3.75	3.84	0.286	0.011	−8.76	0.225
^{62}Fe	−8.39	3.93	3.75	3.83	0.189	0.016	−8.69	
^{64}Fe	−8.36	3.98	3.75	3.83	−0.100	−0.003	−8.61	
^{66}Fe	−8.32	4.04	3.76	3.84	0.002	0.000	−8.51	
^{68}Fe	−8.17	4.11	3.78	3.86	0.004	0.000	−8.41	
^{70}Fe	−8.21	4.21	3.85	3.93	0.266	0.186	−8.29	
^{72}Fe	−8.10	4.29	3.89	3.97	0.336	0.239	−8.18	

where $B(E2)\uparrow$ is the reduced electric quadrupole transition rate for the ground state to 2^+ state transition. For better comparing with the experiment, we show the calculated absolute values of β_2 with IQMDD, NL3, and FSU in Fig. 2. Here, we take S, Ar, Cr, and Fe isotopic chains as examples, and then the $|\beta_2|$ obtained with NL3, FSU, and IQMDD and the experimental data [35] are plotted as functions as the neutron number N.

It can be seen in Fig. 2 that some absolute values of the quadrupole deformation calculated with IQMDD are a bit larger than the ones calculated with NL3, FSU, and the experimental values. However, the shapes and changing trends

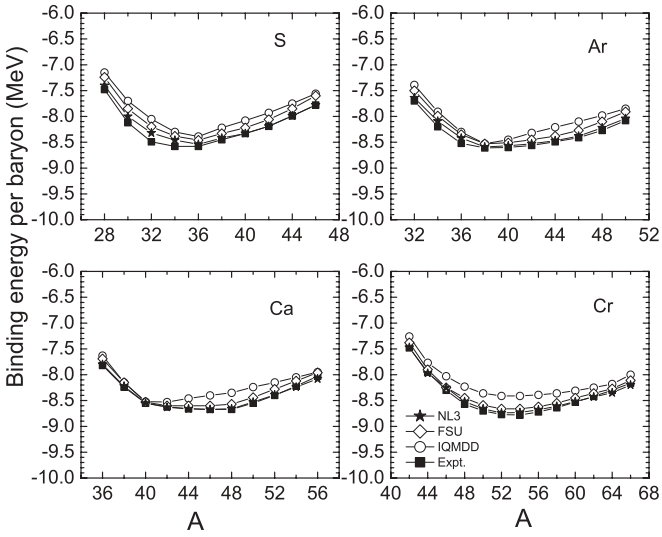

FIG. 1. The calculated binding energy per baryon and the experimental data taken from Ref. [34] for S, Ar, Ca, and Cr isotopic chains.

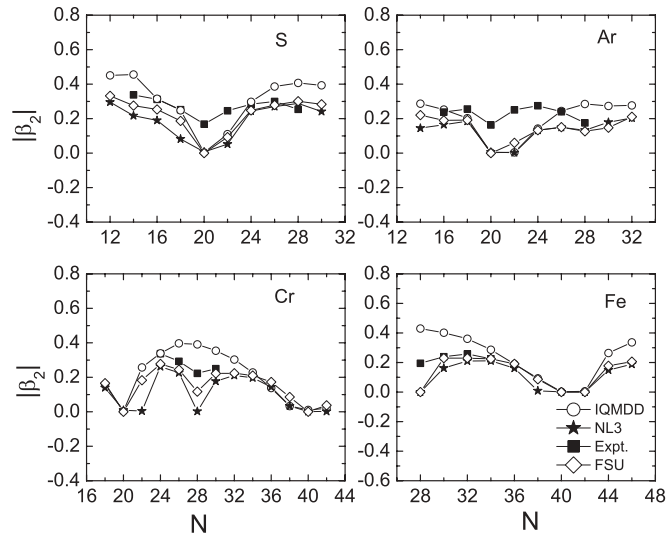

FIG. 2. The calculated absolute values of quadrupole deformation β_2 for S, Ar, Cr, and Fe isotopic chains obtained with IQMDD, FSU, and NL3. The available experimental data are also included for comparison.

TABLE II. Energy difference (in MeV) and associated deformations for nuclei with possible shape coexistence in the ground-state with IQMDD.

Nucleus	$E_{\rm pro} - E_{\rm obl}$	β_2(pro)	β_2(obl)
^{30}Si	−0.034	0.447	−0.374
^{28}S	−0.869	0.451	−0.352
^{30}S	−0.178	0.456	−0.380
^{38}S	−0.067	0.110	−0.094
^{44}S	−0.889	0.407	−0.335
^{46}S	−0.402	0.393	−0.340
^{48}S	0.301	0.371	−0.329
^{42}Ar	0.153	0.142	−0.142
^{44}Ar	0.010	0.244	−0.206
^{46}Ar	0.332	0.285	−0.253
^{54}Ti	−0.366	0.205	−0.176
^{56}Ti	0.361	0.137	−0.156
^{58}Ti	0.322	0.040	−0.091
^{42}Cr	0.233	0.159	−0.151
^{58}Cr	0.265	0.228	−0.215
^{60}Cr	0.549	0.138	−0.154
^{60}Fe	−0.430	0.286	−0.245
^{62}Fe	0.197	0.189	−0.182
^{64}Fe	0.317	0.052	−0.100

of the theoretical curves obtained by IQMDD are similar to those of the experimental results. It is worthwhile to note that the calculated results with IQMDD, NL3, and FSU show that the shapes of ^{36}S and ^{38}Ar are spherical, while the experiment results show that they have quadrupole deformation with β more than 0.15. Meanwhile, it can be seen from Table I that the calculated quadrupole deformation of the Ca isotopic chain also shows the same phenomena. The even-even nuclei from ^{38}Ca to ^{48}Ca are spherical as calculated with IQMDD and NL3 [17], while the experimental β values of these nuclei are more than 0.1. Though the β value provides a useful guide to the nuclear potential deformation, the β and β_2 values differ somewhat [35]. The relationship between β and β_2 may need more discussion.

The shape coexistence is a common phenomenon in deformed nuclei. Our calculation shows that in some nuclei the differences in binding energies between oblate and prolate solutions are very small, which indicates that these nuclei may have shape coexistence in ground state. In Table II, we list the nuclei whose binding energy differences between prolate and oblate minima are less than 1 MeV. Our calculations also show that the shape coexistence nuclei are able to exist close to the spherical nuclei. For instance, the shape of ^{40}Ar is spherical as calculated with IQMDD and NL3 [17], and then the neighbor nuclei ^{42}Ar,^{44}Ar, and ^{46}Ar have shape coexistence by theoretical calculation. The same phenomena can also be seen in Ti and Fe isotopic chains, for the nuclei ^{60}Ti and ^{66}Fe are spherical as calculated with IQMDD and NL3.

The two neutron and two proton separation energies (S_{2n} and S_{2p}) are also very important for describing the nuclei properties and testing the stability of a model. The separation energies can be obtained as the following combinations of

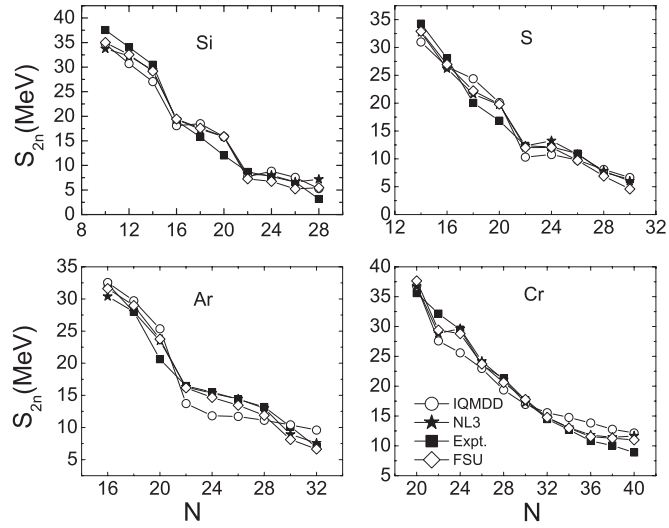

FIG. 3. The two-neutron separation energies S_{2n} for Si, S, Ar, and Cr isotopic chains. The squares, stars, diamonds, and open circles denote the results of the experimental values and the values with NL3, FSU, and IQMDD, respectively.

atomic masses [34]:

$$S_{2n} = -M(A, Z) + M(A-2, Z) + 2\mathrm{n}, \quad (24)$$

$$S_{2p} = -M(A, Z) + M(A-2, Z-2) + 2^1\mathrm{H}. \quad (25)$$

The results with IQMDD and the experimental values taken from Ref. [34] are shown in Figs. 3 and 4. For comparison, the results calculated with NL3 and FSU are also included in the two figures. It can be clearly seen from Fig. 3 that the two-neutron separation energies are getting smaller with increasing neutron number N, and the calculated results with NL3,

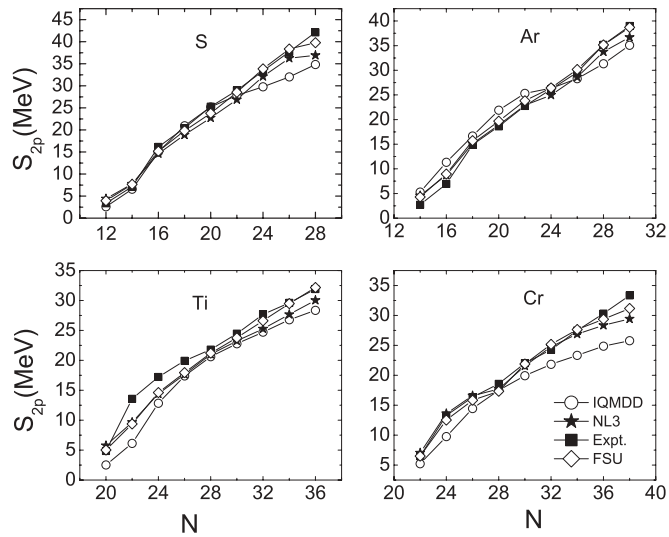

FIG. 4. The two-proton separation energies S_{2p} for S, Ar, Ti, and Cr isotopic chains. The squares, stars, diamonds, and open circles denote the results of the experimental values and the ones with NL3, FSU, and IQMDD, respectively.

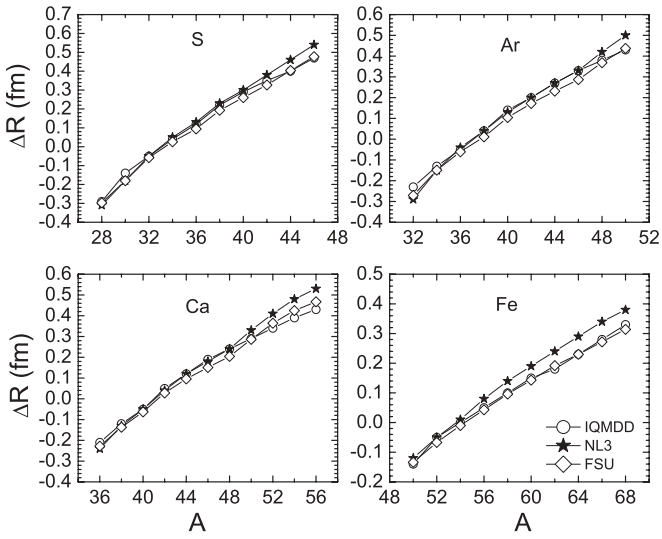

FIG. 5. The neutron skin thickness ($\Delta R = R_n - R_p$) of S, Ar, Ca, and Fe isotopic chains with NL3, FSU, and IQMDD, respectively.

FSU, and IQMDD are all in agreement with the experimental data. In contrast, it is seen from Fig. 4 that the two-proton separation energies are getting bigger with increasing neutron number N. Except for several Cr isotopes, the calculated values with IQMDD are close to the ones with NL3, FSU, and the experimental data. Besides, for S, Ar, and Cr isotopic chains shown in Fig. 3, both the experimental and theoretical curves have a sudden decline at $N = 20$, which indicates that $N = 20$ is a shell closure. With the two-neutron or two-proton separation energy decreasing, there may exist two-neutron or two-proton radioactivity. Though the two-neutron emission has not yet been observed by experiment, the two-proton emissions of ^{12}O and ^{45}Fe have been observed experimentally [36,37].

The neutron skin thickness for S, Ar, Ca, and Fe isotopic chains with IQMDD, FSU, and NL3 are plotted in Fig. 5. It is seen from Fig. 5 that with the neutron number increasing, the neutron skins display an increasing trend for all the isotopic chains with the NL3, FSU, and IQMDD. Such a behavior has also been predicted by the droplet model [38] and experimentally measured [39]. It can also be seen in Table I that the neutron radii increase with neutron number for all the isotopic chains, while the proton radii just slightly decrease for some light isotopes in all isotopic chains and then slightly increase with the neutron number further increasing. Hence the neutron skins increase with the neutron number for all the isotopic chains, which also reflect the pressure of the symmetry energy [40]. Meanwhile, we can see from Fig. 5 that the neutron skin thicknesses calculated with the IQMDD are close to the results with FSU, and become smaller than the ones with the NL3 with the neutron number increasing for all the isotopic chains.

Finally, we discuss the charge radii and show the calculated and experimental ones [41] in Table III. It can be seen that for most nuclei the calculated charge radii are close to the experimental data. The rms deviation of the charge radii with the IQMDD are about 0.06 fm while the rms deviations of the charge radii for these nuclei in NL3 and FSU are about 0.02 fm. Though the rms deviation of the charge radii with the IQMDD are a bit larger than those with NL3 and FSU, the relative deviation of the charge radii in IQMDD with respect to the experimental data is still less than 2%. In conclusion, the IQMDD model can be used to describe the charge radii of the nuclei.

TABLE III. The charge radii (in fm) for some nuclei near $Z = 20$ in IQMDD, as well as the available experimental data for comparison. Here, $\Delta R_c = R_c^{\rm cal} - R_c^{\rm expt}$.

Nucleus	$R_c^{\rm expt}$	$R_c^{\rm cal}$	ΔR_c	Nucleus	$R_c^{\rm expt}$	$R_c^{\rm cal}$	ΔR_c
^{30}Si	3.13	3.29	0.16	^{44}Ca	3.52	3.48	−0.04
^{32}S	3.26	3.35	0.09	^{46}Ca	3.49	3.50	0.01
^{34}S	3.28	3.33	0.05	^{48}Ca	3.47	3.51	0.04
^{36}S	3.30	3.30	0.00	^{50}Ca	3.51	3.54	0.03
^{34}Ar	3.36	3.42	0.06	^{46}Ti	3.61	3.61	0.00
^{36}Ar	3.39	3.41	0.02	^{48}Ti	3.59	3.63	0.04
^{38}Ar	3.40	3.38	−0.02	^{50}Ti	3.57	3.64	0.05
^{40}Ar	3.43	3.39	−0.04	^{50}Cr	3.66	3.74	0.08
^{46}Ar	3.44	3.49	0.05	^{54}Cr	3.69	3.75	0.06
^{40}Ca	3.48	3.46	−0.02	^{56}Fe	3.74	3.84	0.10
^{42}Ca	3.51	3.47	−0.04	^{58}Fe	3.77	3.84	0.07

IV. SUMMARY

In the present work, the ground-state properties of the isotopic chains near $Z = 20$ have been systemically investigated in the IQMDD model. It is the first time that the deformed relativistic mean-field calculation based on quark and meson degrees of freedom has been applied to study the ground-state properties of these isotopic chains. The deviations between the calculated binding energies and the experimental data are small, and they have the same changing trend with the mass number increasing. Meanwhile, the IQMDD model can successfully reflect the shell effect of the neutron magic number $N = 20$. Except for several Ca and Cr isotopes, the calculated two-neutron and two-proton separation energies in IQMDD are in agreement with the results calculated in NL3 and FSU, as well as the experimental data. The calculated quadrupole deformations are a bit larger than the experimental values for some nuclei, but the shapes and changing trends of the theoretical quadrupole deformation curves are very similar to those of experimental results. According to the comparison with available data in this mass region, we find that the IQMDD model can reproduce the charge radii of the nuclei. Additionally, the neutron skin thicknesses calculated with IQMDD are very close to the results in FSU and become smaller than the ones in NL3 with the neutron number increasing for all the isotopic chains. In conclusion, the IQMDD model can give a reasonable description of the axially deformed nuclei in this region. We note that the IQMDD model is based on an effective nuclear potential that has been fitted to nuclear saturation properties. Further fit to the nuclear surface properties should be taken into account in this model in order to improve the result for finite nuclei. Work on this topic is in progress.

ACKNOWLEDGMENTS

This work was supported by the National Natural Science Foundation of China (Grants No. 11035001, No. 10735010, No. 10975072, No. 11120101005, No. 11175232, and No. 11105072), the 973 National Major State Basic Research and Development of China (Grants No. 2013CB834400, No. 2010CB327803, and No. 2013CB834405), CAS Knowledge Innovation Project No. KJCX2-SW-N02, Research Fund of Doctoral Point Grant No. 20100091110028, the Project Funded by the Priority Academic Program Development of Jiangsu Higher Education Institutions (PAPD), and the Science and Technology Development Foundation of Macau (Grant No. 068120111A).

[1] P. Ring, Prog. Part. Nucl. Phys. **37**, 193 (1996); **46**, 165 (2001).
[2] G. A. Lalazissis, J. König, and P. Ring, Phys. Rev. C **55**, 540 (1997); G. A. Lalazissis and P. Ring, Phys. Lett. B **427**, 225 (1998); G. A. Lalazissis *et al.*, *ibid.* **671**, 36 (2009).
[3] B. G. Todd-Rutel and J. Piekarewicz, Phys. Rev. Lett. **95**, 122501 (2005); J. Piekarewicz, Phys. Rev. C **73**, 044325 (2006).
[4] F. J. Fattoyev, C. J. Horowitz, J. Piekarewicz, and G. Shen, Phys. Rev. C **82**, 055803 (2010).
[5] Z. Z. Ren, A. Faessler, and A. Bobyk, Phys. Rev. C **57**, 2752 (1998); Z. Z. Ren, F. Tai, and D. H. Chen, *ibid.* **66**, 064306 (2002).
[6] Z. Q. Sheng, Z. Z. Ren, and W. Z. Jiang, Nucl. Phys. A **832**, 49 (2010).
[7] P. A. M. Guichon, Phys. Lett. B **200**, 235 (1988).
[8] K. Saito, K. Tsushima, and A. W. Thomas, Prog. Part. Nucl. Phys. **58**, 1 (2007).
[9] D. P. Menezes, P. K. Panda, and C. Providencia, Phys. Rev. C **72**, 035802 (2005); P. Wang, R. K. Su, H. Q. Song, and L. L. Zhang, Nucl. Phys. A **653**, 166 (1999).
[10] P. Papazoglou, S. Schramm, J. Schaffner-Bielich, H. Stocker, and W. Greiner, Phys. Rev. C **57**, 2576 (1998).
[11] P. Wang, Z. Y. Zhang, Y. W. Yu, R. K. Su, and H. Q. Song, Nucl. Phys. A **688**, 791 (2001); P. Wang, D. B. Leinweber, A. W. Thomas, and A. G. Williams, *ibid.* **744**, 273 (2004); P. Wang, V. E. Lyubovitskij, T. Gutsche, and A. Faessler, Phys. Rev. C **67**, 015210 (2003); P. Wang, A. W. Thomas, and A. G. Williams, *ibid.* **75**, 045202 (2007).
[12] P. Wang, D. B. Leinweber, A. W. Thomas, and A. G. Williams, Nucl. Phys. A **748**, 226 (2005); P. Wang, H. Guo, Z. Y. Zhang, Y. W. Yu, R. K. Su, and H. Q. Song, *ibid.* **705**, 455 (2002); P. Wang, D. B. Leinweber, A. W. Thomas, and A. G. Williams, Phys. Rev. C **70**, 055204 (2004).
[13] H. Shen and H. Toki, Nucl. Phys. A **707**, 469 (2002).
[14] C. Wu, W. L. Qian, and R. K. Su, Phys. Rev. C **72**, 035205 (2005); **77**, 015203 (2008); C. Wu and R. K. Su, J. Phys. G: Nucl. Part. Phys. **36**, 095101 (2009).
[15] K. Saito and A. W. Thomas, Phys. Lett. B **327**, 9 (1994).
[16] T. D. Lee, *Particle Physics and Introduction to Field Theory* (Harwood Academic, New York, 1981).
[17] G. A. Lalazissis, S. Raman, and P. Ring, At. Data Nucl. Data Tables **71**, 1 (1999).
[18] Z. Z. Ren, Z. Y. Zhu, Y. H. Cai, and G. O. Xu, Phys. Lett. B **380**, 241 (1996).
[19] R. J. Furnstahl, C. E. Price, and G. E. Walker, Phys. Rev. C **36**, 2590 (1987).
[20] S. K. Patra, C. L. Wu, C. R. Praharaj, and R. K. Gupta, Nucl. Phys. A **651**, 117 (1999).
[21] J. P. Maharana, Y. K. Gambhir, J. A. Sheikh, and P. Ring, Phys. Rev. C **46**, R1163 (1992).
[22] G. N. Fowler, S. Raha, and R. M. Weiner, Z. Phys. C **9**, 271 (1981).
[23] G. X. Peng, H. C. Chiang, B. S. Zou, P. Z. Ning, and S. J. Luo, Phys. Rev. C **62**, 025801 (2000); P. Wang, *ibid.* **62**, 015204 (2000); Y. Zhang, R. K. Su, S. Q. Yin, and P. Wang, Europhys. Lett. **53**, 361 (2001).
[24] A. Manohar and H. Georgi, Nucl. Phys. B **234**, 189 (1984).
[25] B. R. Serot and J. D. Walecka, Internat. J. Modern Phys. E **6**, 515 (1997).
[26] C. Wu and R. K. Su, J. Phys. G: Nucl. Part. Phys. **35**, 125001 (2008).
[27] C. Wu, W. L. Qian, Y. G. Ma, G. Q. Zhang, and S. Kumar, Europhys. Lett. **98**, 21001 (2012).
[28] C. Wu and Z. Z. Ren, J. Phys. G: Nucl. Part. Phys. **37**, 105110 (2010).
[29] Y. Zhang, W. L. Qian, S. Q. Ying, and R. K. Su, J. Phys. G: Nucl. Part. Phys. **27**, 2241 (2001).
[30] Y. K. Gambhir, P. Ring, and A. Thimet, Ann. Phys. (NY) **198**, 132 (1990).
[31] P. Möller and J. R. Nix, Nucl. Phys. A **536**, 20 (1992).
[32] P. Möller, J. R. Nix, W. D. Myers, and W. J. Swiatechi, At. Data Nucl. Data Tables **59**, 185 (1995).
[33] S. K. Patra, S. Yoshida, N. Takigawa, and C. R. Praharaj, Phys. Rev. C **50**, 1924 (1994).
[34] G. Audi, A. H. Wapstra, and C. Thibault, Nucl. Phys. A **729**, 337 (2003).
[35] S. Raman *et al.*, At. Data Nucl. Data Tables **78**, 1 (2001).
[36] R. A. Kryger *et al.*, Phys. Rev. Lett. **74**, 860 (1995).
[37] J. Giovinazzo *et al.*, Phys. Rev. Lett. **89**, 102501 (2002).
[38] W. D. Myers, *Droplet Model of Atomic Nuclei* (Plenum, New York, 1977).
[39] A. Trzcinska, J. Jastrzebski, P. Lubinski, F. J. Hartmann, R. Schmidt, T. von Egidy, and B. Klos, Phys. Rev. Lett. **87**, 082501 (2001).
[40] M. B. Tsang *et al.*, Phys. Rev. C **86**, 015803 (2012).
[41] I. Angeli, At. Data Nucl. Data Tables **87**, 185 (2004).